NASA TECHNICAL MEMORANDUM

NASA TM X-72634

COPY NO.

NASA TM X-72634

EXPERIMENTAL MEASUREMENTS OF SKIN FRICTION ON AN UPPER SURFACE BLOWN WING

By Dennis D. Miner and James F. Campbell

January 3, 1975

NATIONAL AERONAUTICS AND SPACE ADMINISTRATION

LANGLEY RESEARCH CENTER, HAMPTON, VIRGINIA 23665

1. Report No.	2. Government Accession No.	3. Recipient's Catalog No.
NASA TM X-72634		

4. Title and Subtitle	5. Report Date
EXPERIMENTAL MEASUREMENTS OF SKIN FRICTION ON AN UPPER SURFACE BLOWN WING	January 3, 1975
	6. Performing Organization Code
7. Author(s)	8. Performing Organization Report No.
Dennis D. Miner and James F. Campbell	
	10. Work Unit No.
9. Performing Organization Name and Address	
NASA Langley Research Center Hampton, Virginia 23665	11. Contract or Grant No.
	13. Type of Report and Period Covered
12. Sponsoring Agency Name and Address	High-Number TM X-
National Aeronautics and Space Administration Washington, D. C. 20546	14. Sponsoring Agency Code

15. Supplementary Notes

Special technical information release, not planned for formal NASA publication.

16. Abstract

An experimental investigation was conducted to obtain skin-friction measurements on a wing with a circular jet exhausting above it. A Preston tube was used to determine the local shear stress at a point on the wing's upper surface. Data were obtained for four nozzle pressures and four vertical displacements of the jet above the wing. The results indicated that the highest skin-friction values occurred with the jet closest to the wing and with the highest nozzle pressure. These data trends were validated by calculations which combined two-dimensional, turbulent boundary-layer theory with axisymmetric co-flowing jet theory.

17. Key Words (Suggested by Author(s)) (STAR category underlined)	18. Distribution Statement
Aerodynamics Upper surface blowing Preston tube	Unclassified-Unlimited

19. Security Classif. (of this report)	20. Security Classif. (of this page)	21. No. of Pages	22. Price*
Unclassified	Unclassified	39	$3.75

*Available from { The National Technical Information Service, Springfield, Virginia 22151
STIF/NASA Scientific and Technical Information Facility, P.O. Box 33, College Park, MD 20740

NATIONAL AERONAUTICS AND SPACE ADMINISTRATION

EXPERIMENTAL MEASUREMENTS OF SKIN FRICTION ON AN UPPER SURFACE BLOWN WING

By Dennis D. Miner and James F. Campbell
Langley Research Center
Hampton, Virginia

SUMMARY

An experimental investigation was carried out to obtain skin friction measurements on a wing with a circular jet exhausting above it. A Preston tube was used to determine the local shear stress at a point on the wing's upper surface. Data were obtained at four different jet nozzle pressures and four different vertical displacements of the jet above the wing.

Results of this study showed that, for a given nozzle pressure ratio, the largest C_f values occurred with the jet closest to the wing, and decreased as the jet vertical distance was increased. Increases in the nozzle pressure ratio increased C_f; this effect was greatest when the jet was close to the wing but diminished as the jet was raised, until, at 2 jet diameters above the wing there was no effect.

Calculations of skin friction were made using a two-dimensional, turbulent, boundary-layer theory to estimate local skin friction, and an axisymmetric co-flowing jet theory to approximate local flow conditions. With the jet closest to the wing surface, reasonable estimates of C_f were obtained when the jet's longitudinal velocity decay was accounted for. The decrease in C_f, that resulted when the jet was raised, was estimated by a mass conservation theory which accounted for the jet's lateral velocity decay. Although the theories did not predict the measured values of C_f exactly, the agreement was close enough to validate the data trends.

INTRODUCTION

One of the current developments in STOL technology under study at NASA is the concept of Upper Surface Blowing (USB), which is implemented by locating jet engines above the airplane wings. This has the aerodynamic advantages of shielding engine noise as well as producing high lifts necessary for STOL operation (Ref. 1).

One of the problems with USB configurations is the scrubbing drag that results from the interaction of the jet exhaust with the wing surface. This is not a serious problem at landing or takeoff because this type of drag is small compared to lift-induced drag. But at cruise, where the scrubbing drag becomes a higher percentage of the total drag, performance penalties will result. This fact is demonstrated in References 1 and 2. Since there are little data available to establish the severity of this potential problem, it is desirable to obtain some experimental skin friction measurements to determine the effect of geometric design variables.

Hence, this present investigation was undertaken to measure local skin friction on a swept, three dimensional wing with a circular jet exhausting above it. A Preston tube system, such as that described in References 3 and 4, was used to determine the local shear stress at a point on the wing's upper surface. This information was then used to calculate the local skin friction coefficient. An attempt was then made to validate experimental trends with trends established by calculations using flat plate boundary layer theory.

Data were taken for jet nozzle total pressures of 0, 4, 8, and 14 PSIG with the jet exit positioned at the wing's leading edge. The vertical location of the jet was varied from 0.5 to 2.0 nozzle exit diameters above the wing chord plane, which was at zero angle-of-attack. The tests were conducted in Langley's 7- by 10-foot wind tunnel at a freestream Mach number of 0.15.

SYMBOLS

a	speed of sound (ft/sec)
a_*	reference speed of sound (ft/sec)
A	reference area (ft^2)

C	wing chord (in)
C_f	local coefficient of friction referenced to freestream conditions, $\tau_w/1/2\ \rho_\infty\ V_\infty^2$
C_f^*	local coefficient of friction referenced to local conditions, $\tau_w/1/2\ \rho_\ell\ V_\ell^2$
d_i	inside diameter Preston tube (in)
d_o	outside diameter Preston tube (in)
$d_{o_{MAX}}$	maximum outside diameter Preston tube (in) (See Appendix A)
$d_{o_{MIN}}$	minimum outside diameter Preston tube (in) (See Appendix A)
D	diameter of jet nozzle exit (in)
g	gravity constant, 32.2 (ft/sec^2)
M	Mach number
P	static pressure (PSF)
P_t	total pressure (PSF)
q	dynamic pressure(PSF)
r	jet exit radius (in)
R_j	radius of the considered cross-section of the main region of the jet as defined in Figure 5.16 of Ref. 6 (in)
R.N.	Reynold's number referenced to freestream
R_x	Reynold's number referenced to local conditions
R^*	gas constant, 1716 ($ft^2/sec^2-°R$)
T	static temperature (°R)
T_t	total temperature (°R)
V	velocity (ft/sec)
X	reference length (L.E. to Preston tube = 0.724 ft)
Z	vertical distance from wing chord plane to jet centerline (in)
ρ	density $\left(\frac{lbs\text{-}sec^2}{ft^4}\right)$
μ	viscosity ($lbs\text{-}sec/ft^2$)
ν	kinematic viscosity (ft^2/sec)
τ	shear stress (lbs/ft^2)

γ ratio of specific heats, 1.4 for air

Subscripts

i	average in inner region of jet
K	maximum after lateral decay on wing surface
ℓ	local
M	maximum after longitudinal decay on jet centerline
N	jet exit
o	average in outer region of jet
p	Preston tube
s	wing static port
w	wall
∞	free stream

MODEL DESCRIPTION AND APPARATUS

Wing

Figure 1 shows the geometry of the 3-D semi-span wing. The root chord of the wing had a NACA 64A008 airfoil section and the tip chord had a NACA 64A006 section. A reflection plate was attached 8.086 inches from the root, leaving a wing having a 17.1 inch semi-span with an aspect ratio of 7.25. To insure turbulent flow on the model, a transition strip of #80 grit was applied 1/2 inch back (in streamwise direction) from the leading edge on the upper surface only (see Fig. 2).

Preston Tube and Jet in Relation to Wing

Figure 2 shows the Preston tube, static port, and the air jet positions relative to the wing. The tip of the Preston tube was located at 3.0625 inches from the reflective plate and 8.688 inches from the leading edge. This position represents an X/C of approximately 80 percent. The jet nozzle lip was located at the leading edge and was moved vertically for various test conditions. As noted in Figure 2, the vertical distance (Z) is measured from the wing chord plane to the nozzle centerline.

Preston Tube Set-Up

Figure 3 presents a close-up of the Preston tube which is a circular cross section surface tube for measuring total pressure in the boundary layer. Because the pressures measured by a Preston tube are sensitive to tube diameters, calculations (from Ref. 3) for minimum and maximum tube outside diameters led to a choice of 0.063 inch for an outside diameter (d_o). The inside diameter (d_i) was 0.043 inches, giving an inside to outside diameter ratio of 0.68. Since these calculations were based on V_∞, the case also had to be checked to see if the tube sizes would be appropriate when V_N was at its maximum value. In this case it was, since the limits for $d_{o_{MIN}}$ and $d_{o_{MAX}}$ are very broad.

The tube was mounted as shown so that the tube leading edge was firmly in contact with the wing surface (see Fig. 3).

Previous measurements obtained by the Preston tube technique have been for two-dimensional or axisymmetric flow fields. In fact, the Preston tube calibrations reported in Refs. 3 and 4 were acquired using two-dimensional flat plates. Therefore, there are uncertainties about using a Preston tube on a finite wing, which can have spanwise velocity gradients. This problem is alleviated somewhat by the insensitivity of total pressure tubes to local flow angularity. In an effort to minimize this problem area for the present tests, the Preston tube was located close to the wing root (i.e., reflection plane), where there would be very little spanwise flow to influence the measurements.

Jet Nozzle Set-Up

The one-inch circular orifice air jet is shown in Figure 4. A total pressure probe (differential pressure gage) and a temperature probe (chromel-alumel thermocouple) were mounted inside the jet. A static pressure probe was located on the centerline of the nozzle at the exit plane for calibration runs only. The jet flow was generated by a high-pressure air system (up to 600 PSI maximum), which provided a continuous supply of dry air.

TUNNEL ARRANGEMENT AND PROCEDURE

This investigation was conducted in the Langley high speed 7- by 10-foot tunnel, which is a continuous flow facility. Figure 5 shows a front view of the test section with the wing mounted on the side wall without the jet set-up. Figure 6 shows a sketch of the jet mounted in the tunnel in proximity of the wing. Actual photographs of the model and jet are shown in Figure 7.

Tests were made at a "q_∞" of 33 PSF at zero angle of attack. Freestream Mach number was 0.15 producing a unit Reynolds number of about 1.0×10^6 per foot.

Data collected includes:

1) $P_{t,p}$ - total pressure measured by Preston tube
2) P_s - static pressure taken from wing static port
3) $T_{t,\infty}$ - freestream total temperature (measured by an iron-constantan thermocouple)
4) Jet Nozzle Properties
   A) $T_{t,N}$ - total temperature
   B) P_N - static pressure
   C) $P_{t,N}$ - total pressure

If the jet flow expands isentropically to the jet exit, the usual expression for the jet-exit velocity can be shown to be:

$$V_N = \sqrt{\frac{2\gamma}{\gamma-1} gR^* T_{t,N} \left[1 - \left(\frac{P_N}{P_{t,N}} \right)^{\frac{\gamma-1}{\gamma}} \right]} \qquad (1)$$

For a subsonic, convergent jet, the exit static pressure (P_N) should be equal to the freestream static. In order to determine this, a calibration was made for P_N as a function of nozzle total pressure ratio and the results are presented in Figure 8. The data shows that $P_N \approx P_\infty$ over most of the range of $P_{t,N}/P_\infty$, some differences occurring as the jet approaches a sonic condition, $\left(P_{t,N}/P_\infty\right)_{SONIC} = 1.9$. The values of V_N in Table I obtained from Eq. 1 with $P_N = P_\infty = 2090$ PSF.

Table I lists the measured and calculated jet nozzle conditions for the four jet pressure ratios. The jet-off condition corresponds to $P_{t,N}/P_\infty = 1.0$.

Table I

$P_{t,N}/P_\infty$	M_N	V_N ft/sec	$T_{t,N}$ °F	$P_{t,N}$ PSFA
1.00	.15	171	85.0	2126
1.29	.62	669	61.4	2705
1.57	.83	886	54.6	3282
2.00	1.04	1045	49.8	4148

The main concern of this investigation was the determination of local skin friction coefficient for various jet nozzle total pressures (hence flow rates) and for various displacements of the jet above the wing. Table II shows the various configurations tested (X). The Z/D value of 0.5 corresponds to the condition where the bottom of the jet is down on the wing.

Table II

Z/D \ $P_{t,N}/P_\infty$	1.00	1.29	1.57	2.00
0.5	X	X	X	X
1.0	X	X	X	X
1.5	X	X	X	X
2.0	X	X	X	X

Thus the reduced data would show the variation of the skin friction for changes in jet nozzle pressures for various vertical displacements above the wing.

DATA REDUCTION

Using Ref. 4 as a guide, a computer program was written to handle the recorded data and calculate skin friction coefficients. The data obtained through this procedure are presented in Table III.

Table III

Z/D	$P_{t,N}/P_\infty$	$P_{t,p}$ PSFA	P_s PSFA	$P_{t,\infty}$ PSFA	T_t^* °F	C_f
0.5	1.00	2119.3	2093.2	2127.3	85.0	.0057
0.5	1.29	2431.3	2095.6	↓	61.4	.0432
0.5	1.57	2633.6	2098.7	↓	54.6	.0577
0.5	2.00	2940.3	2102.7	↓	49.8	.0743
1.0	1.00	2116.0	2092.9	2127.0	82.6	.0050
1.0	1.29	2282.8	2095.1	↓	82.0	.0280
1.0	1.57	2419.7	2098.6	↓	82.0	.0409
1.0	2.00	2667.3	2101.9	↓	83.0	.0593
1.5	1.00	2116.6	2093.9	2127.6	85.0	.0050
1.5	1.29	2165.3	2093.4	↓	↓	.0124
1.5	1.57	2239.6	2094.2	↓	↓	.0212
1.5	2.00	2371.0	2097.4	↓	↓	.0330
2.0	1.00	2115.6	2092.4	2127.0	88.0	.0051
2.0	1.29	2112.5	2091.7	↓	88.0	.0043
2.0	1.57	2112.4	2092.6	↓	89.0	.0038
2.0	2.00	2112.5	2091.5	↓	89.0	.0037

*See assumption #1 following.

Several assumptions were made concerning the data and its reduction:

1) When the jet was at its lowest vertical displacement (Z/D = 0.5), the local temperature was considered to be the measured jet total temperature, $T_{t,N}$. All other Z/D positions involve the use of freestream temperature, $T_{t,\infty}$.

2) All temperatures were corrected for Mach number.

3) The static pressure, measured at the static port, existed at the Preston tube.

From this data and assumptions, the local speed of sound, density, viscosity, and kinematic viscosity were calculated at the wall:

$$a_w = \sqrt{7/5\ R^* T_t}$$

$$\rho_w = P_s/R^*T_t$$

$$\mu_w = 2.27 \frac{T_t^{3/2}}{T_t + 198.6} \times 10^{-8}$$

$$\nu_w = \mu_w/\rho_w$$

where μ_w is calculated by Sutherland's viscosity law.

The following equation (Eq. 6 in Ref. 4) was used to calculate the shear stress at the wall (τ_w):

$$\frac{\Delta P}{\tau_w} = 96 + 60\left(\log_{10} \frac{u_\tau d_o}{\nu_w}\right) + 23.7\left(\log_{10} \frac{u_\tau d_o}{50\ \nu_w}\right)^2 + 10^4\ M_\tau^2 \left[\left(\frac{u_\tau d_o}{\nu_w}\right)^{0.26} - 2\right] \qquad (2)$$

where $\Delta P = P_{t,p} - P_s$

$$u_\tau = \sqrt{\tau_w/\rho_w}$$

$$M_\tau = u_\tau/a_w$$

This calibration equation (Eq. 2) was developed for compressible boundary layers with pressure gradients and adiabatic conditions.

Two limits have been given for Eq. 2. One, $u_\tau d_o/\nu_w$ should be between 50 and 1000 and two, M_τ should lie between 0 and 0.1. Only one data point in this experiment failed to satisfy both these constraints. The condition of ($P_{t,N}/P_\infty = 2.0$) and ($Z/D = 0.5$) produced a $u_\tau d_o/\nu_w = 1543.98$. However, it met the M_τ condition and thus this data point was believed to be close enough to the limitations to be included in the results.

Figure 9 shows a flow chart of the program used in calculating the shear stress. Since τ_w in Eq. 2 could not be solved for directly, a rough value for τ_w was chosen and both sides of Eq. 2 were calculated and compared. If the difference was within ±.001, the program used this value of τ_w in calculating C_f.

If the difference was greater than ±.001, an increment was added to τ_w and the process repeated. This continued until the "correct" τ_w was found.

C_f was then calculated from the following equation using τ_w:

$$C_f = \tau_w / \frac{1}{2} \rho_\infty V_\infty^2 \tag{3}$$

where ρ_∞ and V_∞ were freestream values of density and velocity.

DISCUSSION OF EXPERIMENTAL RESULTS

Since a few assumptions were made concerning the data reduction, the main emphasis was toward trends established by the investigation.

Figure 10 is a plot of skin friction coefficient (C_f) vs. nozzle pressure ratio ($P_{t,N}/P_\infty$) and Figure 11 is a plot of skin friction coefficient (C_f) vs. vertical nozzle displacement (Z/D). Together, these plots show two trends:

1) For a given vertical nozzle displacement, the higher the nozzle pressure ratio, the higher the skin friction coefficient. Both figures show this conclusion. In addition, skin friction increases more rapidly with increases in $P_{t,N}/P_\infty$ for the condition where the nozzle is closest to the wing. In Figure 10 for example, with Z/D = 0.5, the initial pressure jump from 1.0 to 1.29 $P_{t,N}/P_\infty$ produces the largest increase in skin friction; increasing Z/D progressively decreases this effectiveness.

2) For any nozzle pressure ratio, the highest skin friction values are obtained with the jet closest to the wing. Figures 10 and 11 both show this conclusion. Figure 11, in particular, shows that as the jet position is raised to Z/D = 2.0, the skin friction decreases to approximately the value of skin friction obtained with the jet off (i.e., $P_{t,N}/P_\infty = 1.0$). Thus the further away the jet is from the wing surface, the less effect it has on the skin friction of that wing section.

Looking at Table III (data listing) and Figure 11 for Z/D = 2.0, it appears that increasing nozzle pressure actually decreases the skin friction. One possible reason for this trend is that the jet flow is scavenging some of the total pressure being measured by the Preston tube.

THEORETICAL SKIN FRICTION ESTIMATES

Since there appears to be no available theory that can calculate the complicated viscous interaction between wing and jet flow fields, a basic two-dimensional, flat plate boundary layer theory from Reference 5 was used in an effort to validate the experimental data trends. Of course, how well the flat plate assumptions approximate the actual flow conditions depends on a variety of factors. Some of the most important factors are:

1) The two-dimensional nature of the flow near the wing's surface, which is influenced by wing planform and section geometries.

2) The definition of the local flow conditions on the wing's surface, which is dependent on the relative positions of the wing and jet, as well as on their respective flow properties.

Schlichting (Ref. 5) on pages 599-600 provides a method of calculating local skin friction coefficients for flat plates with turbulent boundary layers. Since the test Reynold's numbers (including the jet flow conditions) were between 5×10^5 and 10^7, Eq. 21.12 of Schlichting was used in a modified form; the 1/2 was used in $\tau_w/\rho_\infty V_\infty^2$ to produce $\tau_w/1/2\ \rho_\infty V_\infty^2$ and thus:

$$C_f^* = .0592(R_x)^{-1/5} \tag{4}$$

where $R_x = V_\ell X/\nu_\ell$.

Since the test model wing used a transition strip, the section may not have had a completely turbulent boundary layer, for which Eq. 4 applies. A correction factor was used (Eq. 21.13 of Ref. 5) to account for an initial laminar length. The laminar region was very small however, so that the C_f's for the laminar/turbulent and the all turbulent cases were almost identical.

Thus, the problem to be solved is the definition of the local flow properties; hence R_x. And since the experimental C_f's were referenced to freestream conditions (Eq. 3), C_f^* must be changed to this reference:

$$C_f = \frac{q_\ell}{q_\infty} \frac{\tau_w}{1/2\ \rho_\ell V_\ell^2} = \frac{q_\ell}{q_\infty} C_f^* \tag{5}$$

where the local dynamic pressure, q_ℓ is assumed to act at the boundary layer edge. In the following sections, an attempt is made to define q_ℓ for a variety of jet flow conditions and vertical positions.

Jet Close to the Wing Surface

The first attempt to estimate C_f was for the condition where the jet was located closest to the wing surface; i.e., $Z/D = 0.5$. Of course, it is reasonable to assume that the proximity of the jet to the surface would require that a wall-jet situation exists. This approach leads to the assumption that the jet potential core extends beyond the Preston tube location. Hence, there would be no velocity decay of the jet exhaust and the jet exit properties could be used as the local flow properties.

Table IV gives the C_f^* values calculated using Eq. 4 with the local flow conditions equal to the jet exit properties.

Table IV

M_N	$P_{t,N}/P_\infty$	C_f^*	$\left(M_N/M_\infty\right)^2$	C_f
.15	1.00	.0040	1.0 (jet off)	.0040
.62	1.29	.0029	17.08	.0495
.83	1.57	.0027	30.62	.0827
1.04	2.00	.0025	48.07	.1202

In order to be able to compare these calculations to the measured data, it is necessary to account for the dynamic pressure ratio, q_ℓ/q_∞, in Eq. 5. For the present case where $q_\ell = q_N$:

$$\frac{q_\ell}{q_\infty} = \frac{1/2\ \rho_N V_N^2}{1/2\ \rho_\infty V_\infty^2} = \frac{7/10\ P_N M_N^2}{7/10\ P_\infty M_\infty^2}$$

Using the assumption stated earlier that $P_N = P_\infty$, the dynamic pressure ratio is equivalent to $\left(M_N/M_\infty\right)^2$ and, following Eq. 5, is multiplied times C_f^* to get the C_f values listed in Table IV. These values of C_f are plotted in Fig. 10

(dashed curve) and should be compared to the data obtained with Z/D = 0.5.

Although the predicted trend was similar to the data, i.e., increased C_f with increases in $P_{t,N}/P_\infty$, the theoretical values of C_f were much higher than experiment, particularly at large $P_{t,N}/P_\infty$. The thought now was that the initial assumption about the jet potential core extending to the test station was wrong. Possibly the flow conditions at the Preston tube were not the same as at the jet exit.

Next, an attempt was made to determine the jet potential core length by using the theory of Abramovich (Ref. 6), Eq. 5.20. The estimates obtained from this theory suggest that a reasonable potential core length for a co-flowing axisymmetric jet is approximately 5 to 6 jet diameters, depending on V_N/V_∞.

Even though Abramovich's equation for core length is for an axisymmetric jet and not for a circular jet near a flat plate, Dixon (Ref. 7) on pages 22-25, shows that there is little difference between the velocity decays of the two.

Since the Preston tube was located at 8.7 jet diameters from the jet exit, it can be assumed that there is a jet velocity decay at the test station and that the first approach to C_f prediction is inadequate.

Using Figure 5.19 in Abramovich, it is possible to determine the longitudinal velocity decay in a co-flowing axisymmetric jet. This theory is used to obtain the velocity at the jet centerline, V_M, at a point 8.7 jet exit diameters downstream from the jet exit. Table V gives the values of V_M along with the corresponding values of V_N. Assuming that the local flow properties are determined by V_M, C_f^* and C_f can be calculated by Eqs. 4 and 5, respectively. The values of C_f^* and C_f are listed in Table V, and a sample calculation is provided in Appendix B.

The theoretical values for C_f, which account for a longitudinal velocity decay, are plotted in Figure 10 (dashed curve) and can be compared with the previous estimates obtained with no velocity decay. It can be seen that the curve with velocity decay taken into consideration is much closer to the experimental data where Z/D = 5.0. Since no experimental data were collected at Z/D = 0.0, it is hard to say what the C_f values would be at this condition; however, it does appear that the theory may represent an upper bound for C_f as $Z/D \to 0$.

Table V

$P_{t,N}/P_\infty$	M_N	V_N ft/sec	V_M ft/sec	C_f^*	$\left(M_M/M_\infty\right)^2$	C_f
1.0	.15	171 (jet off)	171	.0040	1.0	.0040
1.29	.62	669	654	.0029	16.3	.0478
1.57	.83	866	796	.0028	25.9	.0700
2.0	1.04	1045	870	.0027	31.4	.0840

The theoretical values of C_f from Table V are also plotted in Figure 11 at Z/D = 0 (solid symbols). These values, along with the data trends at Z/D = .5, suggest that C_f should be a maximum at Z/D = 0.

Jet Removed From the Wing Surface

Having been satisfied that experimental trends for C_f could be predicted by theory for cases when the jet was close to the wing, the next investigation was aimed at prediction of the skin friction coefficient for cases where the jet was elevated above the wing. It is recalled that experimental data were taken for conditions of 0.5, 1.0, 1.5 and 2.0 jet-exit diameters above the wing chord plane. Therefore, in order to estimate the trends of C_f with Z/D, it is necessary to study the lateral velocity decay characteristics for an axisymmetric jet. Using flat plate theory as a basis, the previously stated assumptions concerning the flow were again considered.

The first method used in calculating the lateral decay involved an evaluation of the velocity profile in the main region of the jet. In this region, the velocity profile has stabilized beyond the potential core and can be readily analyzed. Abramovich (Ref. 6, Eq. 5.23) gives an equation for the velocity profile of a co-flowing axisymmetric jet:

$$\frac{V_K - V_\infty}{V_M - V_\infty} = \left[1 - \left(Z/R_j\right)^{1.5}\right]^2 \qquad (6)$$

where this profile is presented in Fig. 12. After the value of the jet radius, R_j, is determined from Figure 5.16 of Abramovich, Eq. 6 can be solved for V_K. Knowing V_K and defining the other flow conditions produces a R_x to be used in Eq. 5 and Eq. 6 for C_f.

This technique led to fair agreement with experimental data when $Z \to 0$ and when $Z \geq R_j$, but for the in-between distances of Z, the C_f values were much lower than the data. This implies that the local velocity used to calculate C_f was too low compared to what the experimental C_f data suggests it should be. This is not surprizing since these calculations take the V_K that would exist laterally at Z from the jet centerline and make no attempt to account for the interaction of the jet flow with the flat plate. In the actual flow, the jet velocity close to the plate would be accelerated because the proximity of the surface reduces the flow "area".

In an effort to account for this effect, a second approach was tried and involved the use of a mass conservation principle. Figure 12 defines the terms applied in this method. The idea is to take a vertical slice through the jet cross-section (Fig. 12b), and to treat the flow in this plane-of-symmetry as if it were two dimensional. By equating the mass flow rate in the outer region $(\rho AV)_o$ to the mass flow rate in the inner region $(\rho AV)_i$ along this plane-of-symmetry, it is possible to get the average flow conditions in the inner region in terms of both the average flow conditions in the outer region as well as R_j/Z. Foss (Ref. 8) on page 40 substantiates that it is possible to use an axisymmetric velocity profile in the outer region of a jet in proximity of a flat plate. Therefore, Eq. 6 was used to describe the velocity profile of the outer region. An integration of this equation was performed, as shown in Eq. 7,

$$V_o = \frac{\int_o^{R_j} V_K \, dr_j}{\int_o^{R_j} dr_j} \tag{7}$$

in order to obtain an expression for the average velocity in the outer region. This yielded,

$$V_o = .55V_\infty + .45V_M \qquad [Z \leq R_j] \tag{8}$$

For $Z \geq R_j$, the integration in Eq. 7 must be carried out with different limits. This results in

$$V_o = (1 - .45\ R_j/Z)V_\infty + .45(R_j/Z)V_M \qquad [Z \geq R_j] \tag{9}$$

If $R_j/Z = 1$, this equation reduces to Eq. 8.

The continuity equation ($\rho_o A_o V_o = \rho_i A_i V_i$) is now used to obtain V_i in terms of V_o and R_j/Z. It is assumed that $\rho_o = \rho_i$, and for $Z \leq R_j$, A_o is considered to be R_j and A_i to be Z. This leads to:

$$V_i = R_j/Z\ V_o \qquad [Z \leq R_j] \tag{10}$$

where V_o is given in Eq. 8.

However, if the flow is symmetric; i.e., $Z \geq R_j$, then there is no interaction of the jet on the plate. For this situation, $A_o = A_i = Z$, which leads to:

$$V_i = V_o \qquad [Z \geq R_j] \tag{11}$$

where V_o is given in Eq. 9.

The average inner-region velocity (V_i) is used to define the local flow properties needed in the flat plate theory to calculate the skin friction coefficient. A sample calculation using this technique is presented in Appendix C, while the C_f results are tested in Table VI for the various test conditions.

Figure 13 shows a plot of C_f vs Z/D, where the lines represent theory, and the symbols represent experimental data. It can be seen from Eq. 10 for the mass conservation theory that as $Z \to 0$, $V_i \to \infty$, and therefore $C_f \to \infty$ as shown in the figure. Of course, this is not physically realistic since there is a maximum nozzle velocity, V_M, as discussed previously, which represents an upper bound to the C_f. The horizontal solid lines, labeled $q_\ell = q_M$, are these upper bounds for the three nozzle pressure conditions and were originally

Table VI

$P_{t,N}/P_\infty$	M_N	C_f (Z/D=.5)	C_f (Z/D=1.0)	C_f (Z/D=1.5)	C_f (Z/D=2.0)
1.29	.62	.086	.023	.014	.011
1.57	.83	.148	.034	.018	.014
2.00	1.04	.25	.058	.027	.020

presented in Table II. In the limit as $Z \to \infty$, the mass conservation approach given by Eqs. 9 and 11, shows that $V_i \to V_\infty$. Thus, the C_f evaluated by the theory approaches that estimated by freestream conditions, labeled $q_\ell = q_\infty$ in Figure 13. The experimental data indicates that, as $Z/D \to 2.0$, the measured C_f values approach the freestream value much faster than the theory estimates.

At intermediate values of Z/D, $.5 < Z/D < 2$, the mass conservation theory gives reasonable estimates of the experimental trends, estimating the effects of both Z/D and $P_{t,N}/P_\infty$.

CONCLUSIONS

An experimental investigation involving Upper Surface Blowing was conducted in Langley's high speed 7- by 10-foot tunnel at a Mach number of 0.15. A Preston tube was used to measure the local skin friction coefficient at a point 8.7 jet exit diameters behind the jet nozzle on a 3-D wing. Four jet pressure ratios and four jet vertical position above the wing were studied. The major results of this investigation can be summarized as follows:

1) For any given jet nozzle pressure ratio, the largest skin friction coefficient values occured with the jet closest to the wing and decreased as the jet vertical distance was increased.

2) For any given jet vertical distance from the wing, increases in the jet pressure ratio led to increases in skin friction coefficient.

3) At a position of 2 jet diameters above the wing, the jet had little or no effect on the skin-friction coefficient.

4) Calculations of skin friction were made using a two-dimensional, turbulent, boundary-layer theory to estimate local skin friction, and an axisymmetric coflowing jet theory to approximate local flow conditions. With the jet closest to the wing surface, reasonable estimates of C_f were obtained when the jet's longitudinal velocity decay was accounted for. The decrease in C_f, that resulted when the jet was raised, was estimated by a mass conservation theory which accounted for the jet's lateral velocity decay. Although the theories did not predict the measured values of C_f exactly, the agreement was close enough to validate the data trends.

APPENDIX

Appendix A.- Preston Tube Size

Reference 3 provides curves for estimating the maximum and minimum Preston tube diameters. They are based on Reynolds number.

$$R.N. = \frac{\rho_\infty V_\infty X}{\mu_\infty}$$

$$T_{t,\infty} = {}^\circ F + 459.6 = {}^\circ R$$

$$\mu_\infty = 2.27 \frac{T_{t,\infty}^{3/2}}{T_{t,\infty} + 198.6} \times 10^{-8} \text{ lbf sec/ft}^2$$

$$\rho_\infty \equiv \text{assumed sea level} = .002378 \frac{\text{lbf sec}^2}{\text{ft}^4}$$

$$V_\infty \equiv \text{freestream} = 171 \text{ ft/sec}$$

$$X \equiv \text{reference length} = .724 \text{ ft (Preston tube from L.E.)}$$

$$T_{t,\infty} = 72^\circ F$$

thus $$\mu_\infty = 3.81 \times 10^{-7} \frac{\text{lb sec}}{\text{ft}^2}$$

$$M_\infty = .15$$

$$R.N. = \frac{(.002378)(171)(.724)}{3.81 \times 10^{-7}} = 773{,}620$$

From Figure 4A in Ref. 3

$$\frac{d_{O_{MAX}}}{X} = 8.5 \times 10^{-3}$$

$$d_{O_{MAX}} = .074 \text{ inch for reference length}$$

From Figure 4B in Ref. 3

$$\frac{d_{o_{MIN}}}{X} = 2.5 \times 10^{-3}$$

$$d_{o_{MIN}} = .022 \text{ inch for reference length}$$

Appendix B.- Longitudinal Velocity Decay Determination

Case: $M_N = .83$

$$V_N = 866 \text{ ft/sec}$$

$$V_\infty = 171 \text{ ft/sec}$$

$$\frac{V_\infty}{V_N} = \frac{171}{866} = .2 = m \text{ (in Abramovich, Ref. 6)}$$

$$\frac{X}{D} = 8.7 \text{ in. } (\frac{\bar{X}}{R_o} \text{ (in Ref. 6)} = 17.4)$$

From Figure 5.19 (Ref. 6):

$$\frac{V_M - V_\infty}{V_N - V_\infty} = \frac{U_M - U_H}{U_o - U_H} \text{ (in Ref. 6)} = .9$$

$$V_M = .9(V_N - V_\infty) + V_\infty = 796.5 \text{ ft/sec}$$

This is the velocity at the Preston tube after a velocity decay.

Assume $T_{t,N} = 514.6°R$

$$a_* = 44.74 \sqrt{T_{t,N}} = 1015 \text{ ft/sec}$$

$$\frac{V_M}{a_*} = \frac{796.5}{1015} = .785$$

$M_M = .758$ from compressible tables

$\frac{T_M}{T_{t,N}} = .897$ from compressible tables

$T_M = 452.3°R$

$\mu_M = .3355 \times 10^{-6} \frac{lbf\ sec}{ft^2}$ from Sutherland's law for viscosity

$\rho_M = \frac{P_N}{R^* T_M} = .00272 \frac{lbf\ sec^2}{ft^4}$

$\nu_M = \mu_M / \rho_M = 1.23 \times 10^{-4}\ ft^2/sec$

Now that all the local properties (M_i) have been defined, C_f can be computed.

$R_x = \frac{V_M X}{\nu_M} = 4.61 \times 10^6$

$C_f^* = .0592\ (R_x)^{-1/5}$ (Eq. 4) $= .00275$ referenced to local condition

To reference this to freestream:

$\frac{q_\ell}{q_\infty} = \left(\frac{M_M}{M_\infty}\right)^2 = \left(\frac{.758}{.15}\right)^2 = 25.54$

$C_f = \left(\frac{q_\ell}{q_\infty}\right)^2 C_f^* = \tau / \frac{1}{2} \rho_\infty V_\infty^2 = .070$

Appendix C.- Mass Conservation Theory for $M_N = .83$

$V_\infty = 171$ ft/sec

$V_M = 796$ ft/sec

$\frac{V_\infty}{V_M} = m$ (used in Ref. 6) $= .215$

From Abramovich (Ref. 6), Fig. 5.19:

$$\frac{V_K - V_\infty}{V_M - V_\infty} \cong \frac{U_M - U_H}{U_O - U_H} \text{ (used in Ref. 6)} = .90$$

$$V_K = .9\,(V_M - V_\infty) + V_\infty = 734 \text{ ft/sec}$$

$X/D = 8.7$ in. or $\bar{x}$ (used in Ref. 6) $= 17.4$

Figure 5.16 (Ref. 6):

$R_j/r = \bar{R}$ (used in Ref. 6) $= 2.6$

$\therefore R_j = 1.3$ in.

For $Z \leq R_j$:

$$V_i = R_j/Z\ V_o$$

where $V_o = .55\ V_\infty + .45\ V_M$

For $Z \geq R_j$:

$$V_i = V_o = (1 - .45\ R_j/Z)\ V_\infty + .45\ R_j/Z\ V_M$$

Flow conditions:

$$T_{t,N} = 514.6°R$$

$$T_{t,\infty} = 545.0°R$$

$$T_{t,i} = \frac{T_{t,N} + T_{t,\infty}}{2} = 529.8°R$$

$$a_* = 44.74 \sqrt{T_{t,i}} = 1030 \text{ ft/sec}$$

A. For the case of Z = 1.0:

Thus, $Z < R_j$

$$\therefore V_o = .55\ (171) + .45\ (734) = 424.4 \text{ ft/sec}$$

and $$V_i = \frac{R_j}{Z} V_o = 551.5 \text{ ft/sec}$$

$$\frac{V_i}{a_*} = .535$$

$$M_i = .50 \text{ from compressible tables}$$

$$\frac{T_i}{T_{t,i}} = .9524 \text{ from compressible tables}$$

$$T_i = 504.6°R$$

$$\mu_i = 3.659 \times 10^{-7} \frac{\text{lbf sec}}{\text{ft}^2} \text{ using Sutherlands law of viscosity}$$

$$\rho_i = \frac{P_{\infty,i}}{R^* T_i} = \frac{2090}{(1716)(504.6)} = .002414 \frac{\text{lb}_f - \text{sec}^2}{\text{ft}^4}$$

$$\nu_i = u_i/\rho_i = 1.52 \times 10^{-4} \text{ ft}^2/\text{sec}$$

$$R_x = \frac{V_i X}{\nu_i} = \frac{(551.5)(.724)}{1.52 \times 10^{-4}} = 2.63 \times 10^6$$

$$C_f^* = \frac{T_w}{1/2\rho_i V_i^2} = \frac{.0592}{(R_x)^{.2}} = 3.08 \times 10^{-3}$$

$$\frac{q_i}{q_\infty} = \left(\frac{M_i}{M_\infty}\right)^2 = 11.11$$

$$C_f = \left(\frac{M_i}{M_\infty}\right)^2 C_f^* = \tau_w/1/2\ \rho_\infty V_\infty^2 = .034$$

B. For the case of Z = 1.5 :

Thus, $Z > R_j$ $\qquad R_j/Z = .8667$

$$V_i = V_o = [1 - .45(.8667)]\ 171 + .45\ (.8667)\ 734$$

$$V_i = 390.6 \text{ ft/sec}$$

$$\frac{V_i}{a_*} = .3792$$

$$M_i = .35 \text{ from compressible tables}$$

$$\frac{T_i}{T_{t,i}} = .9761,\ T_i = 492.5^\circ R$$

$$\mu_i = 3.59 \times 10^{-7}\ \frac{\text{lbf sec}}{\text{ft}^2}$$

$$\rho_i = P_{\infty,i}/R^*T_i = .002473\ \frac{\text{lbs sec}^2}{\text{ft}^4}$$

$$\nu_i = \mu_i/\rho_i = 1.452 \times 10^{-4}\ \text{ft}^2/\text{sec}$$

$$R_x = \frac{V_i X}{\nu_i} = \frac{390.6\ (.724)}{1.452 \times 10^{-4}} = 1.95 \times 10^6$$

$$C_f^* = \frac{.0592}{(R_x)^{.2}} = .00327$$

$$\left(\frac{M_i}{M_\infty}\right)^2 = 5.444$$

$$C_f = .018$$

REFERENCES

1. Putnam, Lawrence E.: Exploratory Investigation at Mach Numbers from 0.40 to 0.95 of the Effects of Jets Blown Over a Wing. NASA TN D-7367, Nov. 1973.

2. Wimpress, John K.: Upper Surface Blowing Technology as Applied to the XC-14 Airplane. SAE (730916), Oct. 1973.

3. Allen, Jerry M.: Critical Preston-Tube Sizes. Journal of Aircraft. Vol. 7, No. 3, May-June, 1970, pp. 285-287.

4. Bradshaw, P.;and Unsworth, K.: A Note on Preston Tube Calibrations in Compressible Flow. IC Aero. Report 73-07, Sept. 1973.

5. Schlichting, Dr. Hermann: Boundary Layer Theory. 1968, pp. 596-601.

6. Abramovich, G. N.: The Theory of Turbulent Jets. 1963, pp. 172-234.

7. Dixon, C. J.; Theisen, J. G.; and Scruggs, R. M.: Theoretical and Experimental Investigations of Vortex Lift Control by Spanwise Blowing. Vol. 1, Experimental Research, Sept. 1973.

8. Foss, John E.; and Kleis, Stanley J.: A Study of the Round-Jet/Plane-Wall Flow Field, Division of Engineering Research, Michigan State University, Oct. 1971.

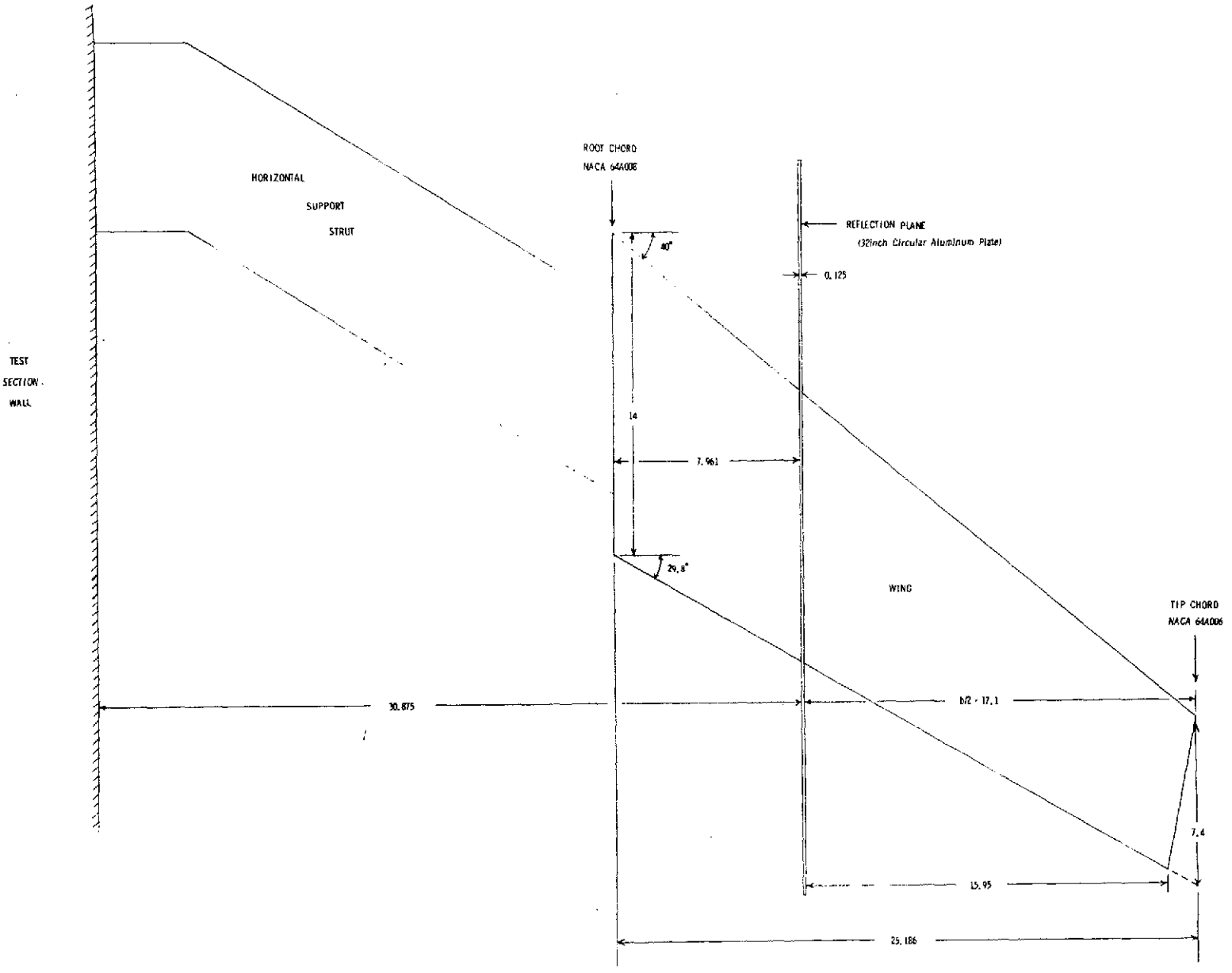

Figure 1. - Wing geometry (all dimensions are in inches).

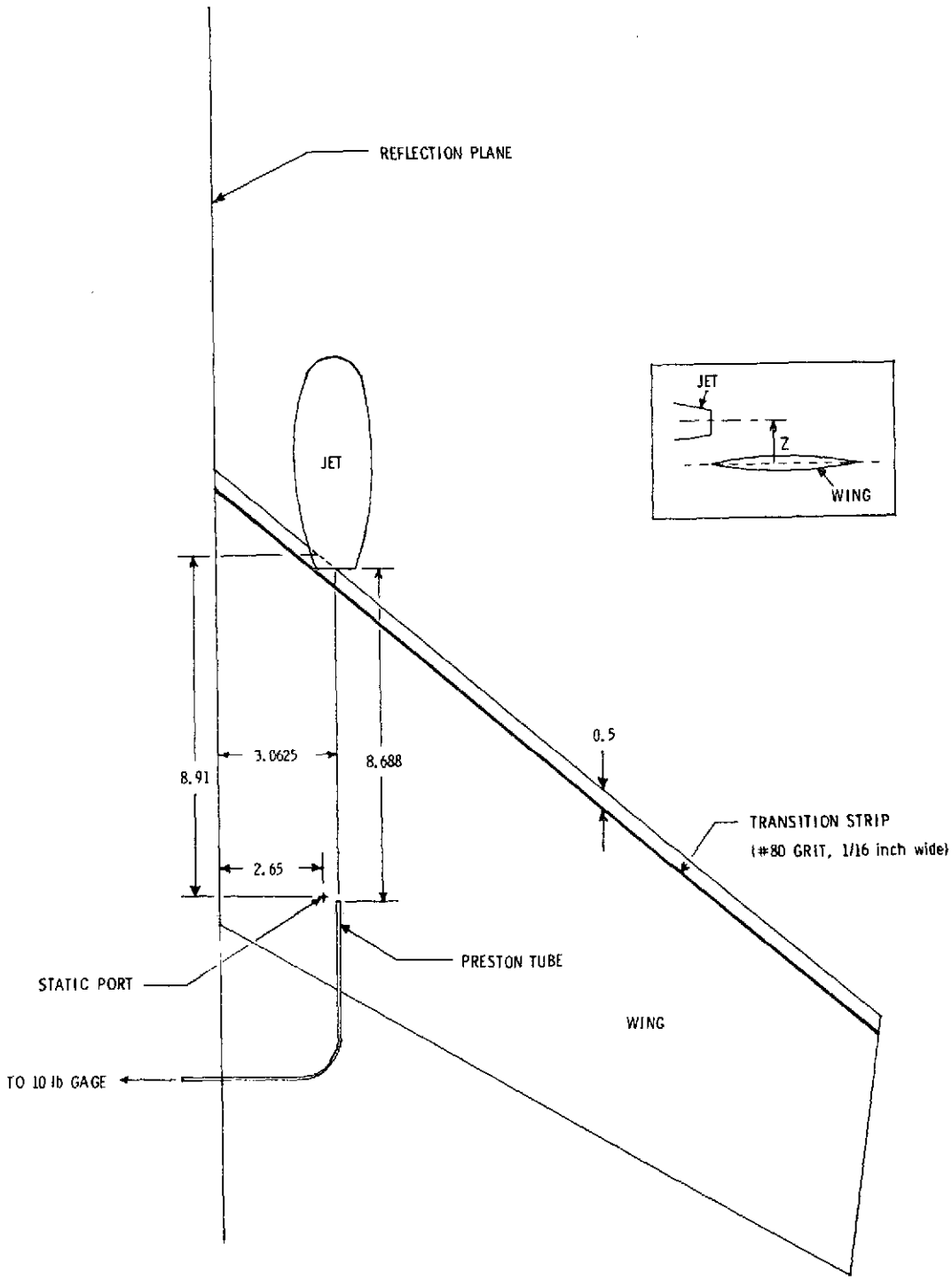

FIGURE 2. JET, PRESTON TUBE, STATIC PORT LOCATIONS
(all dimensions in inches)

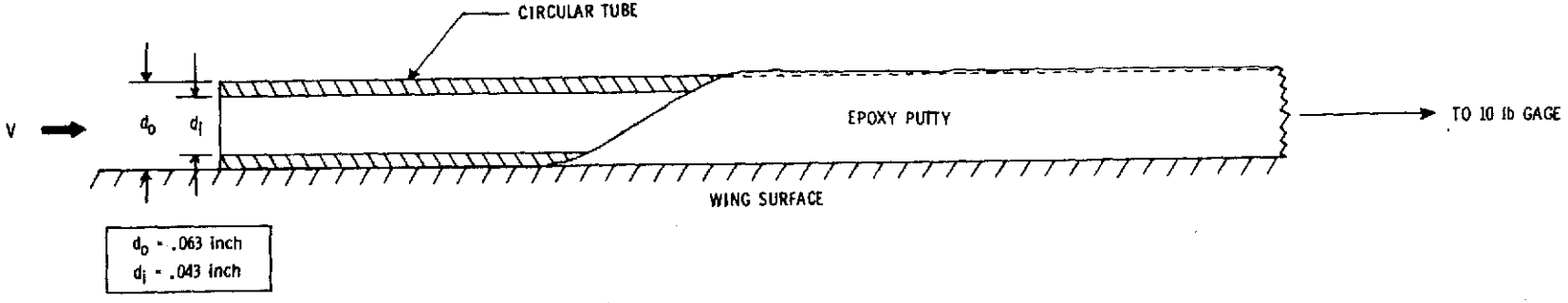

FIGURE 3. PRESTON TUBE

NOZZLE COORDINATES

	Part A	Part B	
X°	R_n	R_{n1}	R_{n2}
0.00	0.000		
0.10	0.343		
0.20	0.473		
0.40	0.644		
0.60	0.761		
0.80	0.848		
1.20	0.968		
1.60	1.040		
2.00	1.077		
2.40	1.087		
3.10	1.052		
3.25		0.850	1.045
3.50		0.830	1.020
3.75		0.790	0.980
4.00		0.750	0.930
4.25		0.695	0.880
4.50		0.640	0.815
4.75		0.580	0.750
4.85		0.560	0.715
4.95		0.540	0.685
5.10		0.520	0.640
5.30		0.500	0.575
5.55		0.500	0.500

coordinates in inches

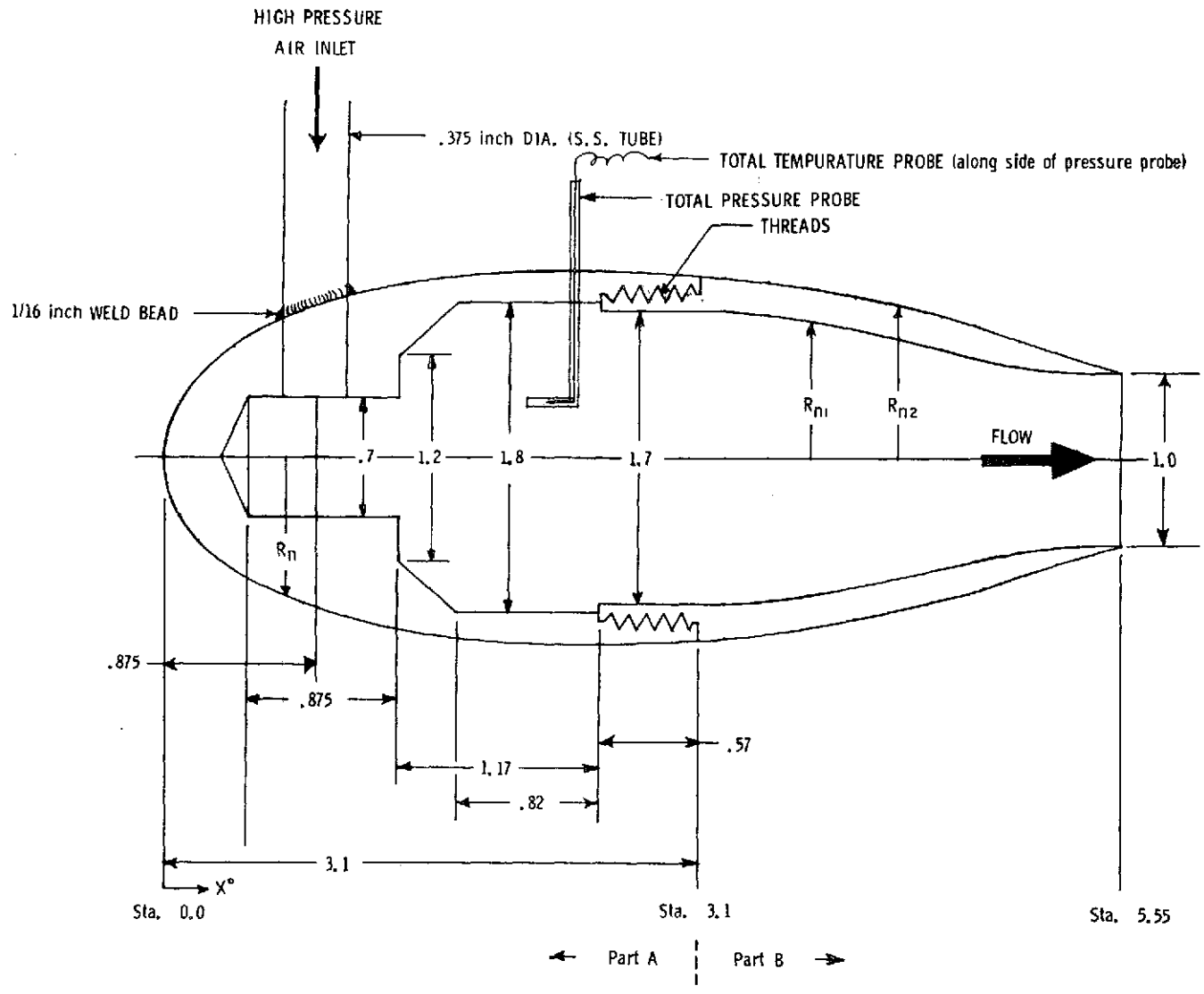

FIGURE 4. JET NOZZLE (all dimensions in inches)

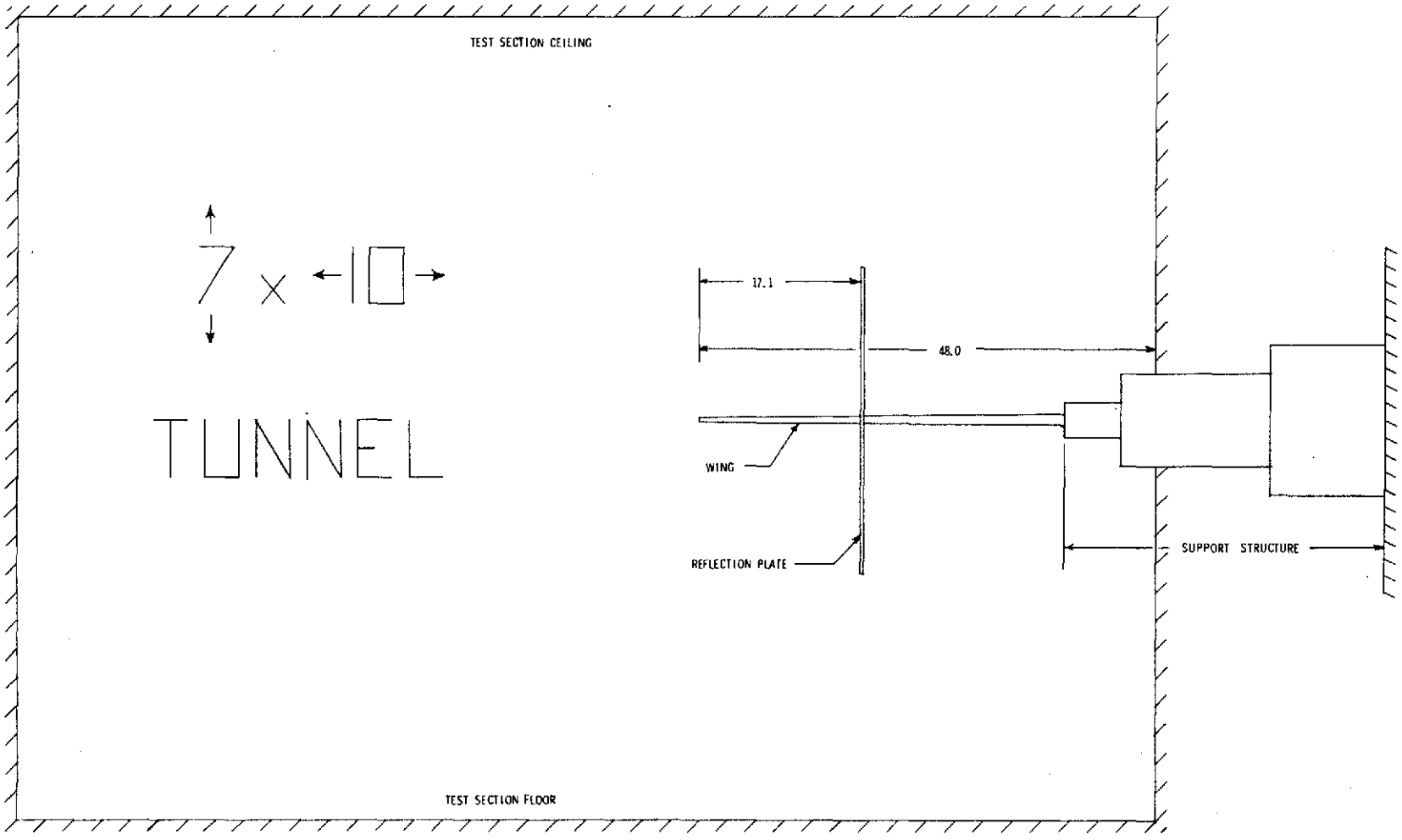

Figure 5. - Front view of tunnel setup (all dimensions in inches).

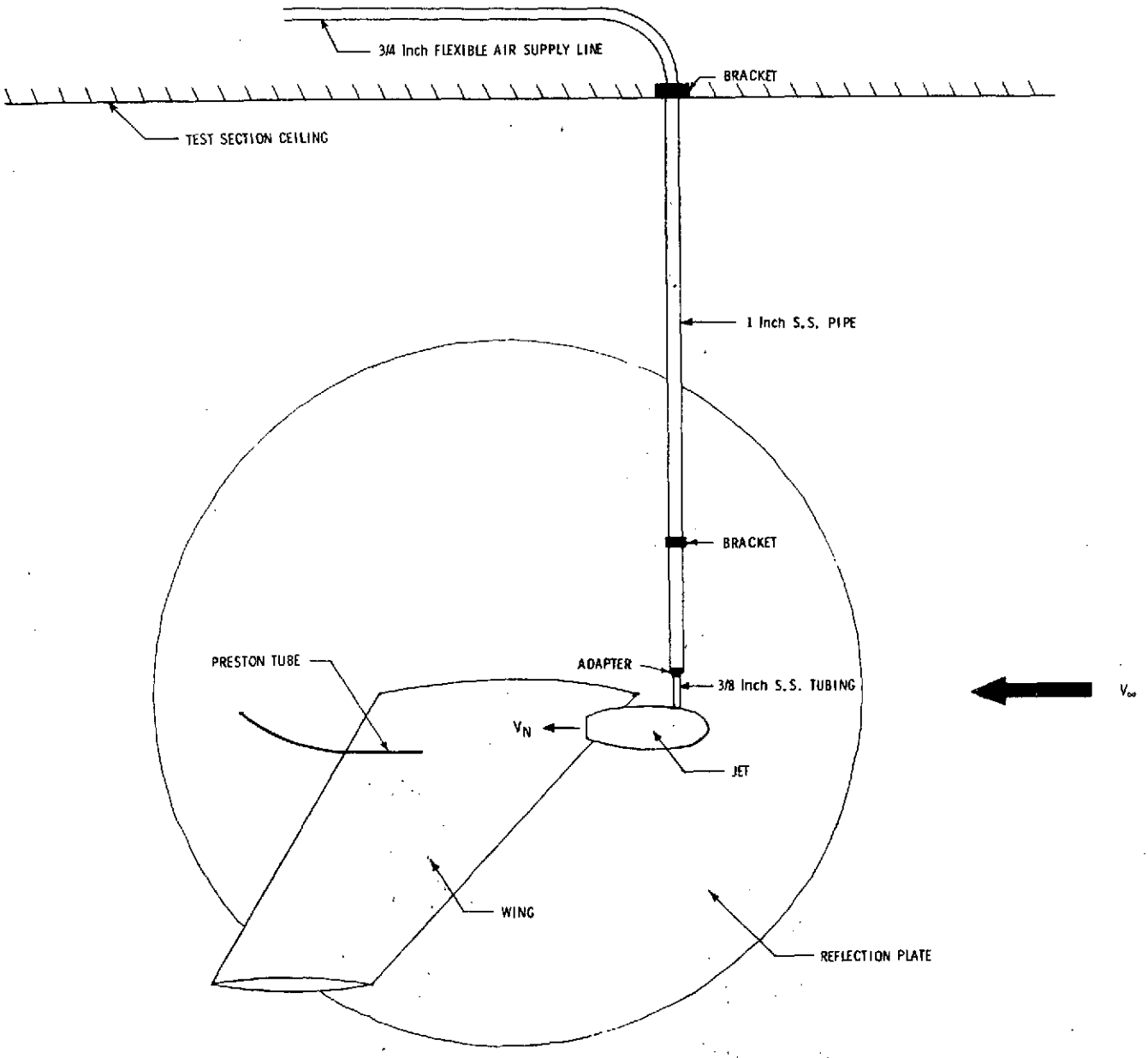

FIGURE 6. SIDE VIEW OF TEST SET-UP (all dimensions in inches).

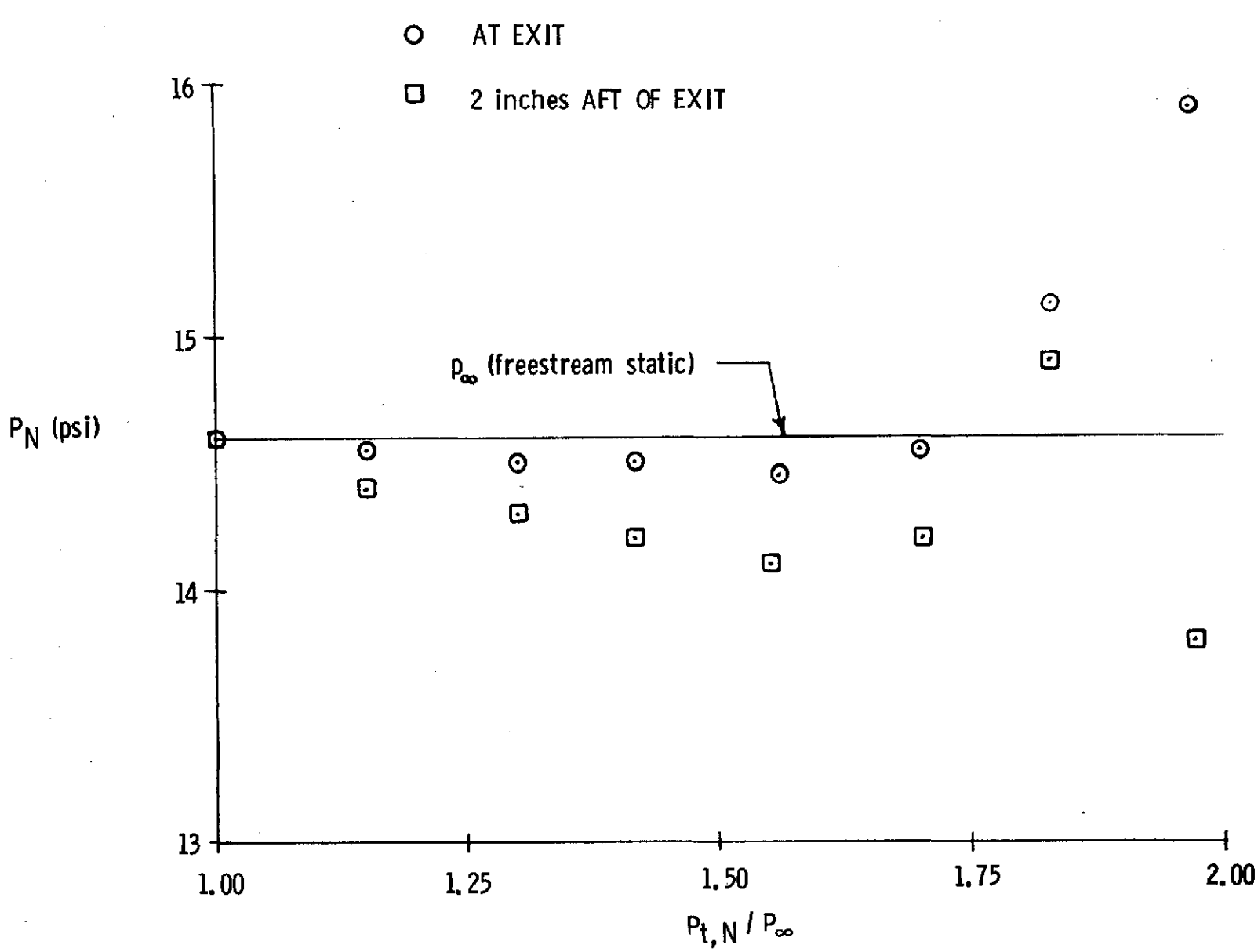

FIGURE 8. NOZZLE TOTAL AND STATIC PRESSURE CALIBRATION, $M_\infty = .15$

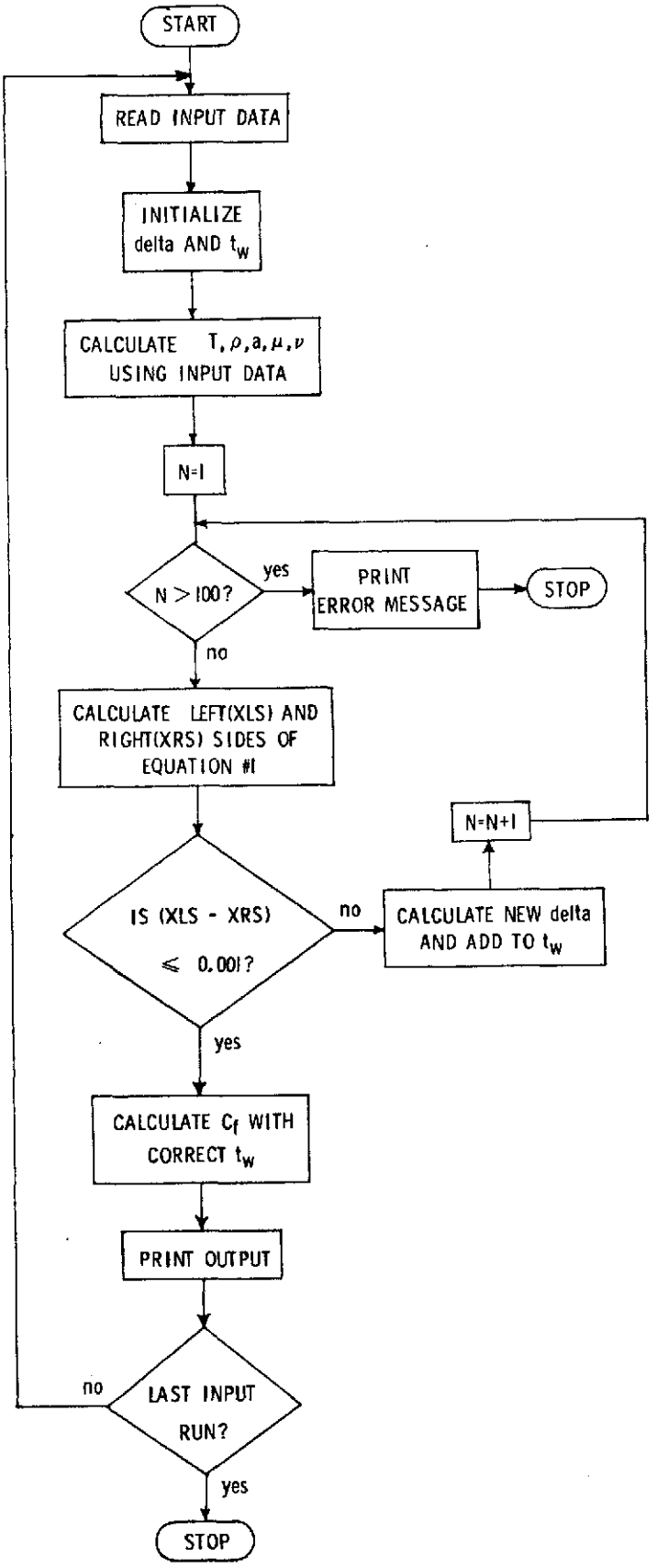

FIGURE 9. FLOW CHART OF COMPUTER PROGRAM FOR DATA REDUCTION

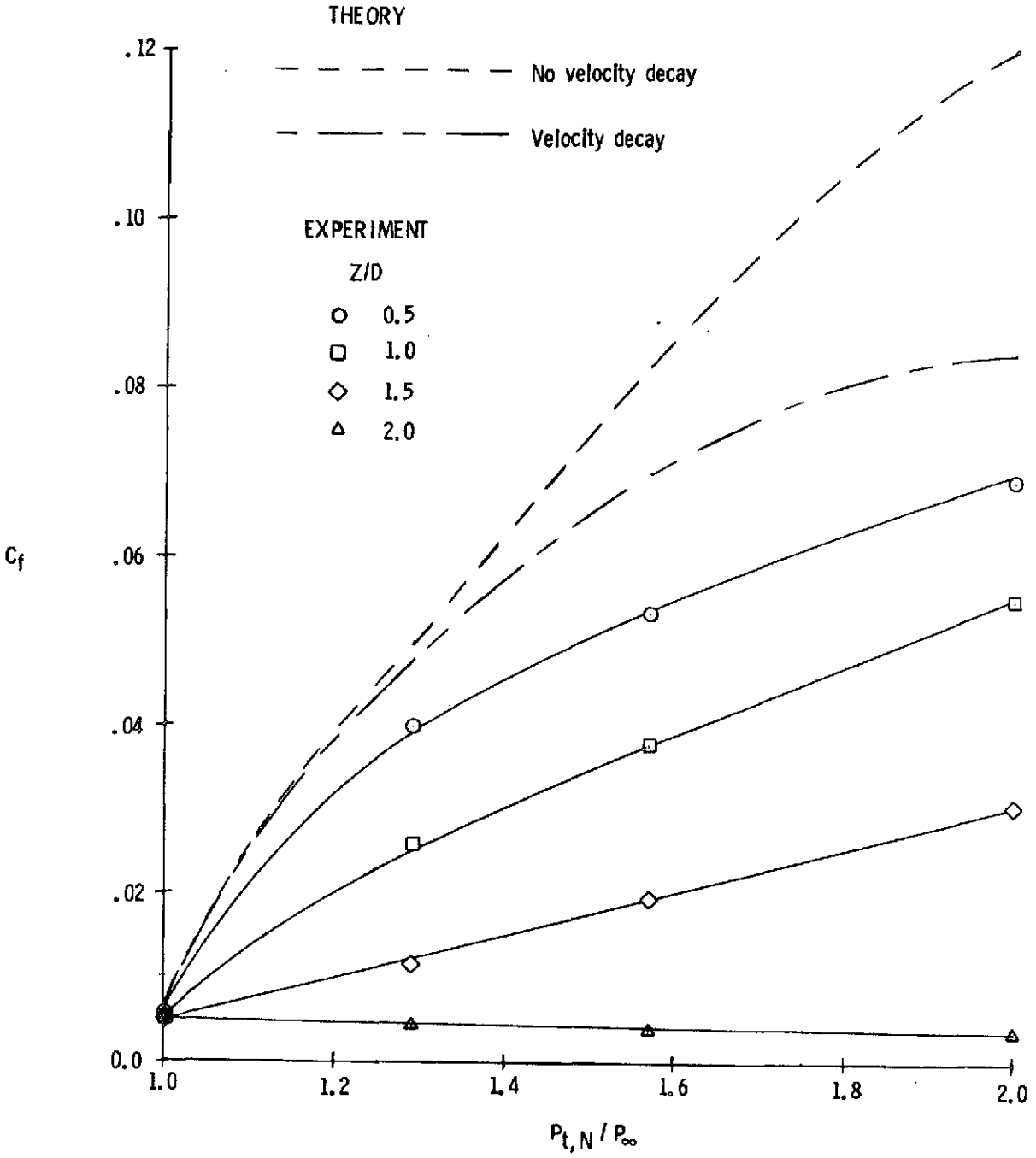

FIGURE 10. EFFECTS OF JET NOZZLE PRESSURE ON C_f FOR VARIOUS JET NOZZLE VERTICAL DISTANCES

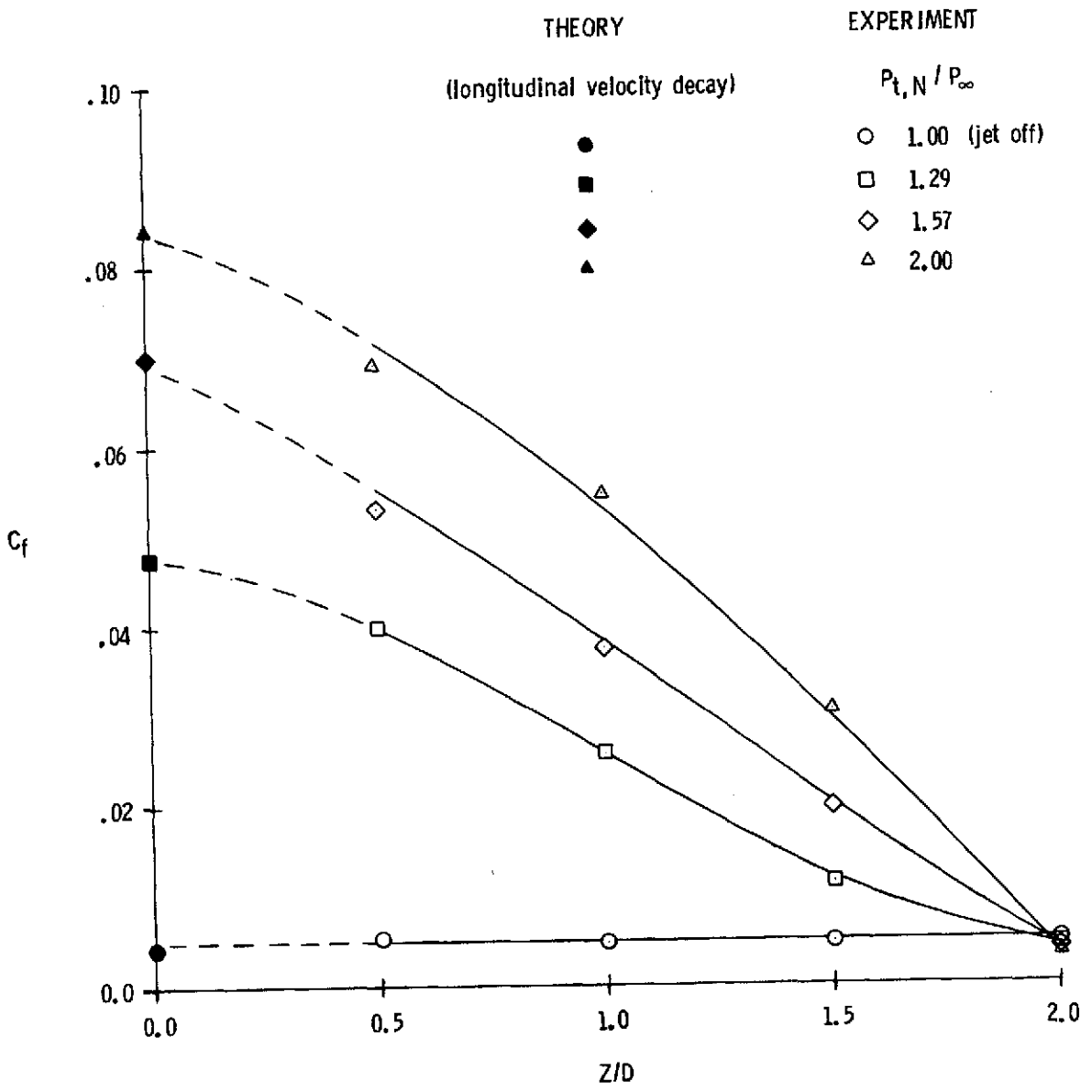

FIGURE 11. EFFECTS OF JET NOZZLE VERTICAL DISTANCES ON C_f FOR VARIOUS JET NOZZLE PRESSURE RATIOS

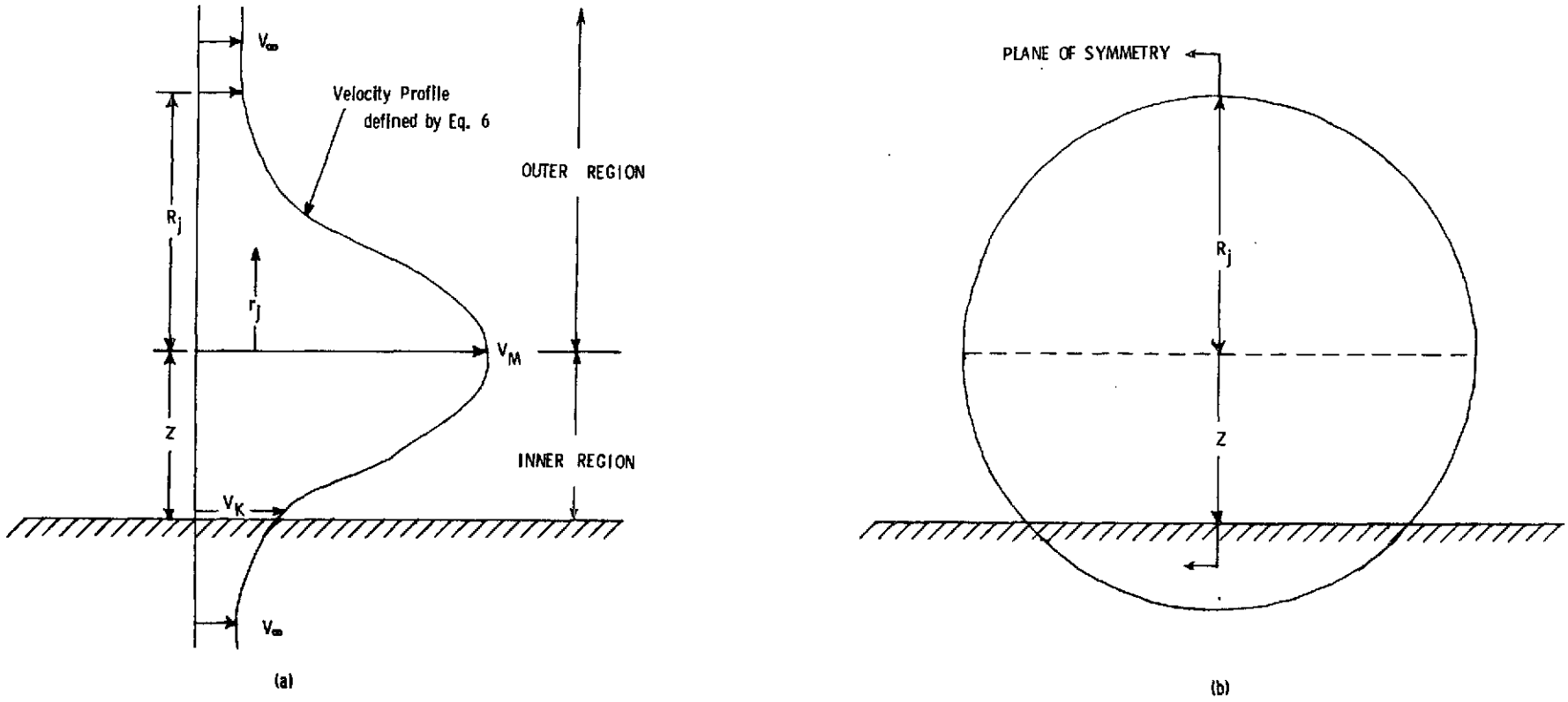

FIGURE 12. SIDE AND FRONT VIEW OF VELOCITY PROFILE

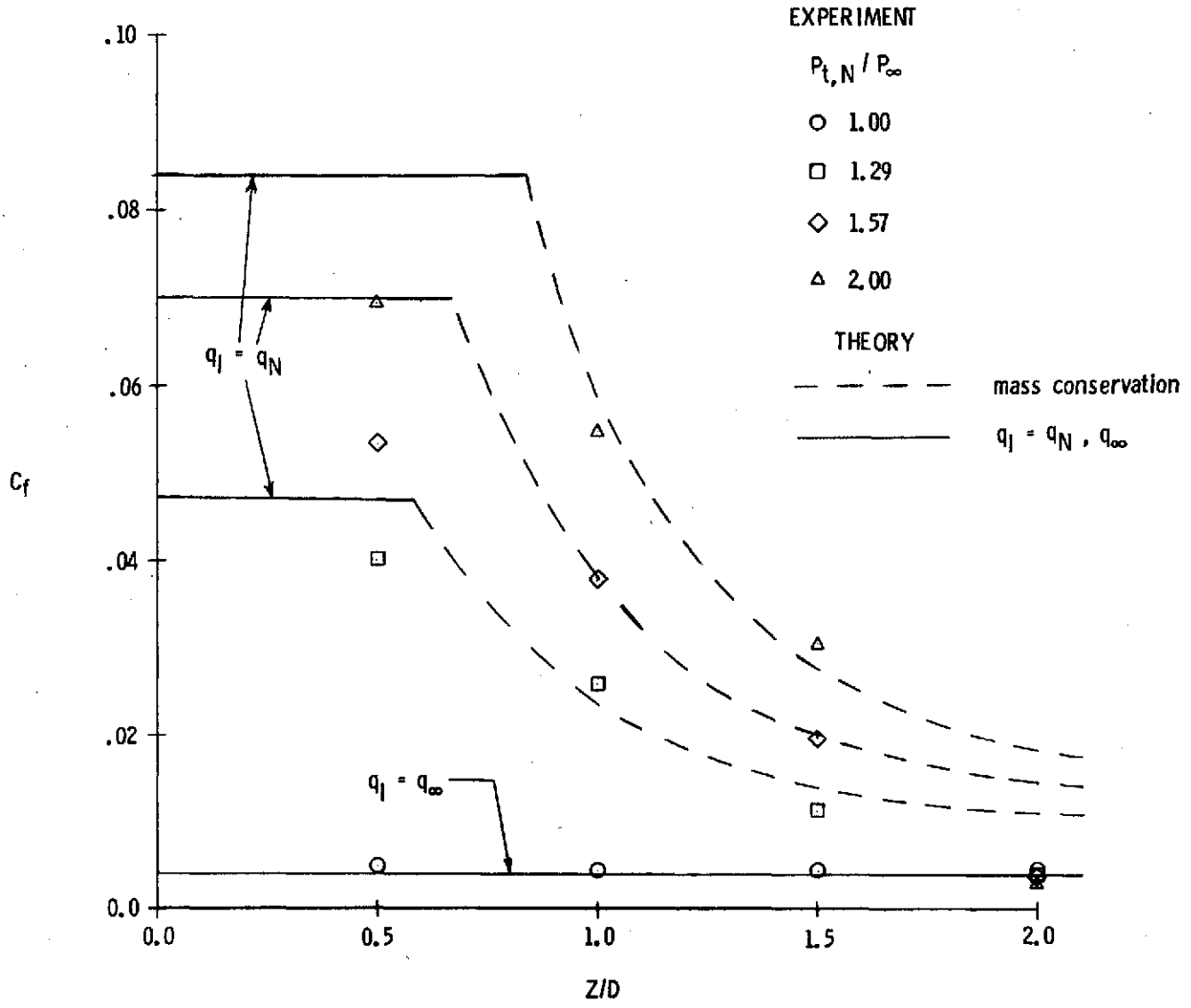

FIGURE 13. COMPARASION OF EXPERIMENTAL AND THEORETICAL EFFECTS OF JET NOZZLE VERTICAL DISTANCE ON C_f FOR VARIOUS JET NOZZLE PRESSURE RATIOS